

# Optimizing Multi-UAV Multi-User System Through Integrated Sensing and Communication for Age of Information (AoI) Analysis

YULIN ZHOU<sup>1</sup> (Member, IEEE), AZIZ ALTAF KHUWAJA<sup>2</sup>, XIAOTING LI<sup>1</sup> (Member, IEEE),  
NAN ZHAO<sup>3</sup> (Senior Member, IEEE), AND YUNFEI CHEN<sup>4</sup> (Senior Member, IEEE)

<sup>1</sup>Ningbo Innovation Center, Zhejiang University, Ningbo 315000, China

<sup>2</sup>Department of Electrical Engineering, Sukkur IBA University, Sukkur 65200, Pakistan

<sup>3</sup>School of Information and Communication Engineering, Dalian University of Technology, Dalian 116024, China

<sup>4</sup>Department of Engineering, University of Durham, DH13LE Durham, U.K.

CORRESPONDING AUTHOR: A. A. KHUWAJA (e-mail: aziz.khuwaja@iba-suk.edu.pk)

This work was supported in part by the Key Research and Development Program of Zhejiang Province under Grant 2023C01043, and in part by the Science and Technology Innovation 2025 Major Project of Ningbo under Grant 2023Z236.

**ABSTRACT** Integrated sensing and communication enhances the spectral efficiency by using shared resources, eliminating the need for separate bandwidth allocations. Unmanned aerial vehicle (UAVs) play a key role in this, offering mobility, flexibility, and extended coverage for serving multiple users, especially in scenarios like disaster response and environmental monitoring. This paper explores multiple UAVs with integrated sensing and communication capabilities, using the Age of Information (AoI) metric to optimize resource allocation for timely data transmission. We propose two algorithms, Variable Particle Swarm Optimization (VPSO) and Twin Variable Neighborhood Particle Swarm Optimization (TVPSO), to jointly optimize power, bandwidth, and UAV trajectories to minimize AoI. Numerical results show the effects of the sensing and communication power ratio, the number of UAVs and the number of users on AoI and energy consumption. Furthermore, TVPSO is shown to outperform other PSO variants and the Deep Q Networks (DQN)-based approach, offering faster convergence and superior performance.

**INDEX TERMS** Age of information, integrated sensing and communication, particle swarm optimization (PSO), resource allocation, and unmanned aerial vehicles.

## I. INTRODUCTION

THE INTERNET of Things (IoT) has driven the development of architectures for data collection, processing, and dissemination, especially in human-centric applications like healthcare and environmental surveillance [1], [2], [3]. The IoT devices monitor physical parameters, such as temperature, humidity, and light intensity, offering periodic system updates [4]. It is predicted that these devices will reach 500 billion by 2025, leading to the massive data generation [5].

Unmanned aerial vehicles (UAVs) are essential for data collection due to their ability to access remote and hazardous areas, provide real-time data, and offer high-resolution imaging and mapping [6], [7]. They ensure precise, cost-effective, and efficient data collection, capable of covering

large areas quickly. UAVs can also carry various sensors, enabling versatile data gathering for applications like agriculture, infrastructure inspection, and environmental monitoring. Additionally, they support frequent, repetitive data collection, essential for time-series analysis and change detection, making them invaluable tools in diverse fields, such as urban planning, disaster response, and smart cities [8], [9].

Real-time location monitoring of ground users using UAVs improves communication performance by enabling adaptive network adjustments, ensuring reliable connectivity, and optimizing data transmission routes based on the precise positions of users in dynamic environments. This data can combine detection and tracking methods by using adjacent frames with shared features to reduce computation time [10]. Traditional real-time location monitoring

by Global Navigation Satellite System (GNSS) provides precise positioning data using satellites [11], but it can face challenges such as signal degradation in urban areas, high latency in dynamic environments, and limited coverage in obstructed or indoor locations, making it less reliable for certain real-time applications. Another approach uses vision-based localization with UAV location and camera angle measurements to estimate target positions in images [12]. However, vision-based methods can suffer from environmental variations and increase power consumption.

Integrated Sensing and Communication (ISAC) has recently gained attention as a key technology for sixth-generation (6G) wireless networks, allowing for the combined use of wireless infrastructure and spectrum resources to deliver both sensing and communication capabilities [13]. It minimizes overheads by integrating sensing and communication functions into unified hardware and signal waveforms [14], [15]. Many studies on ISAC have primarily focused on evaluating performances by maximizing throughput [16], [17], [18]. In [19], UAV-enabled ISAC systems provided various solutions (coordinated interference management and cooperative ISAC) for optimizing the sensing and communication performance. However, these studies overlooked Age of Information (AoI), which is more crucial than traditional rate metrics as it directly reflects data timeliness and relevance, vital for accurate real-time sensing and communication.

Freshness of data, measured by AoI, is crucial in ISAC because it ensures timely and relevant information used in decision-making, reducing the risk of outdated data leading to inefficiencies [20]. Maintaining low AoI allows for more accurate resource allocation and dynamic adjustment. Besides the utilization of information freshness metrics in terrestrial IoT networks [21], many studies have focused on addressing the issue of information freshness in UAV-enabled communication networks. Particularly, in [22], the authors formulated a joint sensing time, transmission time, UAV trajectory, and task scheduling optimization problem. In [23], the authors formulated a joint energy harvesting and data collection time to minimize AoI. In [24], two optimization problems of age-optimal data collection were formulated to minimize the ground sensor nodes' maximal AoI and average AoI. In [25], the authors jointly optimized the UAV trajectory, localization accuracy, bandwidth and beam-width, to guarantee the information freshness. In [26], the authors jointly optimized the visiting sequence for multiple ground targets, number of sensing tasks, trajectory of UAV, service time and transmit power to improve the freshness of the received information at the ground controller. However, these works considered only one UAV in their system models which may not efficiently cover a wide area or handle a large number of users simultaneously, resulting in outdated information for users located farther away from the UAV or during periods of high demand.

Using multiple UAVs reduces AoI by enabling faster and more efficient data updates through distributed coverage

and parallel communication with ground users. In [27], multiple UAVs are used to collect and process data while minimizing the AoI where authors used machine learning (ML) techniques to reformulate the trajectory and scheduling policies problem as a Markov decision process. However, ML techniques, especially deep learning models, require extensive training data and time, whereas particle swarm optimization (PSO) can often provide solutions without such a training phase. Moreover, ML models may struggle to generalize well to new or unseen scenarios, such as sudden change in the number of ground users. Moreover, in [28], a graph theory approach was used to minimize the AoI in multi-UAV assisted IoT network. However, this work relies on simplifications and approximations, which do not fully capture the intricacies of real-world UAV operations.

Heuristic algorithms are beneficial for solving optimization problems and minimizing AoI as they efficiently explore large solution spaces and quickly converge to near-optimal solutions, even in complex and non-linear environments, such as urban areas, disaster zones and agriculture fields. These algorithms are often employed in path planning of multiple UAVs to find near-optimal solutions efficiently, for example, genetic algorithms (GA) in [29], PSO in [30], and ant colony optimization (ACO) in [31].

PSO is a population-based optimization technique inspired by the social behavior of birds flocking or fish schooling, where particles move through the search space to find optimal solutions by adjusting their positions based on their own and their neighbors' experiences [32]. Known for its efficiency in solving complex problems [33], PSO is particularly suitable for multi-UAV and multi-user scenarios. Unlike reinforcement learning methods like Q-learning or DQN, which require extensive training, PSO delivers near-optimal solutions without the need for a training phase, making it ideal for real-time decision-making in UAV path planning. Several PSO variants have been developed to tackle specific challenges: Global best path PSO (GBPSO) for fixed-wing UAVs in adversarial environments [34], spherical-vector-based PSO for improved path planning safety [35], two-swarm learning PSO (TSLPSO) [36], and dynamic group-based collaborative optimization (DGBCO), which adjusts sub-population sizes [37].

Motivated by the above discussion, the main contributions of this work are listed as follows:

- We model integrated sensing and communication in a multi-UAV network serving multiple ground users, where UAVs regularly update sensing data. Unlike [16], [17], [18], we use AoI to measure the time from task initiation to data transmission completion.
- In contrast to studies in [21], [22], [23], [24], [25], [26] that focus on single-UAV systems, we extend the problem to a multi-UAV scenario, formulating an optimization problem for resource allocation and UAV trajectories to minimize the overall AoI. To manage the

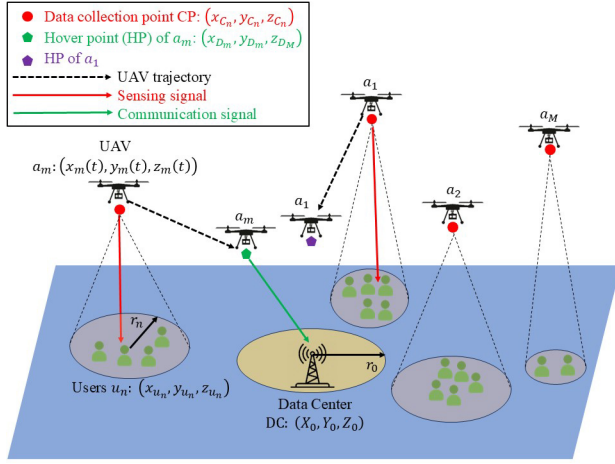


FIGURE 1. System model.

complexity of optimizing multiple variables, we decouple the problem into two sub-problems, simplifying the process while improving resource efficiency and system performance.

- Unlike the PSO-based algorithms in [34], [35], [36], [37], we propose two PSO-based algorithms, Variable neighborhood PSO (VPSO) and Twin variable PSO (TVPSO), for optimizing the trajectories of multiple UAVs.
- We demonstrate that the TVPSO outperform other PSO variants as well as the non-PSO-based DQN approach in terms of the sum of AoI and energy consumption.

The remainder of this article is organized as follows. We present the system model in Section II. The problem formulation of minimizing the AoI while optimizing the resource allocation and flight trajectories of multiple UAVs is given in Section III. The algorithm design is detailed in Section IV. Numerical results are presented in Section V. Finally, we conclude this paper in Section VI.

## II. SYSTEM MODEL

### A. NETWORK DESCRIPTION

Fig. 1 illustrates a multi-UAV, multi-user system with integrated sensing and communication capabilities. The system consists of  $M$  dual-function UAVs, denoted as  $A = \{a_1, a_2, \dots, a_M\}$ , a central data center (DC), and  $N$  users in a set  $U = \{u_1, u_2, \dots, u_N\}$ . Time slots ( $t = 1, 2, \dots, T$ ) are used for UAV sensing and data transmission, with each UAV activity occupying an integer number of time slots. UAVs utilize on-board batteries for sensing and communication.

At time slot  $t$ , the coordinates of UAV  $a_m$  are  $(x_m(t), y_m(t), z_m(t))$ . The DC coordinates are  $(X_0, Y_0, Z_0)$ , and user  $u_n$  position is  $(x_{u_n}, y_{u_n}, z_{u_n})$ . Each user has a sensing area with radius  $r_n$ , denoted as

$$\mathcal{P}_n = \left\{ p = (x, y, z) \mid \sqrt{(x - x_{u_n})^2 + (y - y_{u_n})^2 + (z - z_{u_n})^2} \leq r_n \right\}. \quad (1)$$

Data collection points (CPs)  $C_n$  for each user are located at  $(x_{C_n}, y_{C_n}, z_{C_n})$ , and  $(x_{C_n}, y_{C_n}, z_{C_n}) \in \mathcal{P}_n$ . The set of all data CP coordinates is  $\mathcal{C}_p = \{C_1, C_2, \dots, C_M\}$ .

During sensing, UAVs follow a predefined path, visiting each data CP sequentially. After data collection, they fly to a hover point (HP) near the DC, awaiting data transmission (offloading sensing data) during idle periods. UAVs must satisfy communication range requirements when communicating with the DC. The HP coordinates of UAV  $a_m$  during communication with DC is  $(x_{D_m}, y_{D_m}, z_{D_m})$ . Thus,  $D_m \in \mathcal{P}_0$ , where

$$\mathcal{P}_0 = \left\{ p = (x, y, z) \mid \sqrt{(x - X_0)^2 + (y - Y_0)^2 + (z - Z_0)^2} \leq r_0 \right\}, \quad (2)$$

and  $r_0$  is the radius of the DC's communication range. The set of HP coordinates for all UAVs is  $\mathcal{D}$ .

To manage system complexity and prioritize key components like UAV trajectory, power allocation, and resource management, we chose not to explicitly model the antenna patterns at the UAVs, users, and DC. These aspects will be considered in future research.

### B. SENSING AND COMMUNICATIONS PROTOCOL

In the proposed system, UAV operations are divided into two phases: sensing and communication. During the sensing phase, UAVs collect data from predefined CPs within designated user areas, focusing on interference from other UAVs to simplify the problem by addressing the most significant interference sources in a dynamic UAV network [38]. Although clutter interference is important in real-world scenarios for sensing, its exclusion allows for a more focused analysis on optimizing UAV trajectories, power allocation, and resource management. They can also be considered as the part of the noise in the received signal. After data collection, UAVs transition to the communication phase, moving to HPs near the central DC to transmit the data. Both phases are restricted by energy and transmission rate to ensure optimal performance and resource management.

As depicted in Fig. 2, the finite spectrum resources denoted as  $W$  is divided into  $K$  non-overlapping sub-channels ( $K > M$ ), each occupying  $B = \frac{W}{K}$  bandwidth. The first  $M$  sub-channels of  $K$  are allocated to UAVs as dedicated sensing channels. Each UAV, e.g.,  $a_i$  (where  $i = 1, 2, \dots, M$ ), can focus on one user at a time. Thus,  $\beta_{is_i}$  indicates if the UAV  $a_i$  is sensing user  $u_{s_i}$  (where  $u_{s_i} \in U, s_i \in N$ ) at data CP  $c_{s_i}$ , with  $\beta_{is_i} = 1$  for sensing and  $\beta_{is_i} = 0$  otherwise.

Additionally, to avoid collision between different UAVs communicating with the DC simultaneously, the remaining  $K - M$  sub-channels are allocated for communication between UAVs and the DC. These sub-channels, denoted by the set  $C = 1, 2, \dots, K - M$  ( $K > M$ ), are used for this purpose. A binary variable  $\rho_{v_i c_i}$  ( $v_i \in M, c_i \in C$ ) is defined to represent

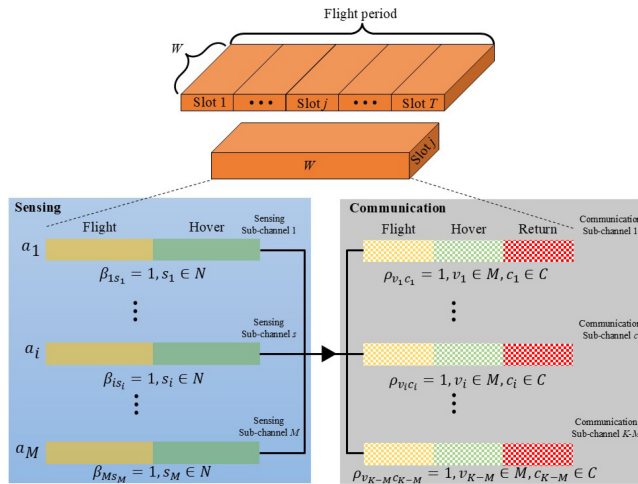


FIGURE 2. Multi-UAV Sensing and Communication.

the allocation of communication channels. Specifically, if the  $c_i$  communication channel is assigned to the UAV  $a_{v_i}$ , then  $\rho_{v_i c_i} = 1$ ; otherwise,  $\rho_{v_i c_i} = 0$ .

In both the sensing and communication phases, AoI is the primary metric guiding UAV operations, balancing energy and transmission rate constraints to maintain data timeliness. During sensing, UAVs optimize their flight paths and CPs to minimize AoI, ensuring quick updates on gathered information. In the communication phase, UAVs prioritize timely data offloading near the central DC, where the transmission rate is managed to conserve energy while keeping data current.

### C. UAV MOBILITY MODEL

Assuming the velocity of the UAV  $a_m$  in time slot  $t$  is  $(v_{mx}(t), v_{my}(t), v_{mz}(t))$ , where,  $v_{mx}(t)$ ,  $v_{my}(t)$ , and  $v_{mz}(t)$  represent the components of the velocity in the  $x$ -direction,  $y$ -direction, and  $z$ -direction, respectively. Velocity components and coordinates are related as  $(v_{mx}(t), v_{my}(t), v_{mz}(t)) = (x_m(t) - x_m(t-1), y_m(t) - y_m(t-1), z_m(t) - z_m(t-1))$ . This relationship is based on the principle of the discrete-time motion of UAVs.

The speed of UAV  $a_m$  is  $v_m = \sqrt{v_{mx}^2 + v_{my}^2 + v_{mz}^2}$ . Considering safety, energy, and structural constraints, UAV speed is constrained as

$$v_{\min} \leq v_m \leq v_{\max} \quad \forall m \in A. \quad (3)$$

Therefore, UAV coordinates have constraints:  $X_{\min} \leq x_m(t) \leq X_{\max}$ ,  $Y_{\min} \leq y_m(t) \leq Y_{\max}$ , and  $Z_{\min} \leq z_m(t) \leq Z_{\max}$ . For the UAV's journey from HP  $D_m$  through data CPs  $C_n$  and back to HP, ensuring operation within the area, constraints are formulated as

$$\begin{cases} X_{\min} \leq x_{C_n} \leq X_{\max}, \\ Y_{\min} \leq y_{C_n} \leq Y_{\max}, \\ Z_{\min} \leq z_{C_n} \leq Z_{\max}, \end{cases} \quad \forall n \in U, \quad (4)$$

and

$$\begin{cases} X_{\min} \leq x_{D_m} \leq X_{\max}, \\ Y_{\min} \leq y_{D_m} \leq Y_{\max}, \\ Z_{\min} \leq z_{D_m} \leq Z_{\max}, \end{cases} \quad \forall m \in A, \quad (5)$$

Maintaining a secure separation between UAVs to avoid collision, constraints for  $a_m$  and  $a_{m'}$  ( $m \neq m'$ ) are governed by their spatial relationship as

$$\sqrt{(x_m - x_{m'})^2 + (y_m - y_{m'})^2 + (z_m - z_{m'})^2} \geq D_{\min}, \quad \forall t \in T, \quad (6)$$

where  $D_{\min}$  is the minimum distance between any two UAVs.

### D. ENERGY MODEL

For each UAV,  $a_m$ , the energy consumption includes hovering energy at the data CP during user sensing phase ( $E_m^{hs}$ ), propulsion energy during UAV flight ( $E_m^f$ ), and hovering energy during communication with the DC ( $E_m^{hc}$ ).

Given the different data transmission rate requirements for sensing and communication, let  $0 < \alpha_m^s < 1$  and  $0 < \alpha_m^c < 1$  represent the fractions of the total power allocated to sensing and communication, respectively, for UAV  $a_m$ . Assume the total power of the UAV during hovering is  $P_m$ . Then, the power allocated to sensing while hovering,  $p_m^s$ , is  $\alpha_m^s P_m$ , and the power allocated to communication while hovering,  $p_m^c$ , is  $\alpha_m^c P_m$ .

The power used to support the UAV's rotor movement in both cases is given by  $p_m^{sz} = (1 - \alpha_m^s) P_m$  for sensing and  $p_m^{cz} = (1 - \alpha_m^c) P_m$  for communication. They must satisfy the energy constraints as

$$\begin{cases} p_m^{sz} \geq p_m^z, \\ p_m^{cz} \geq p_m^z. \end{cases} \quad (7)$$

where  $p_m^z$  denotes the minimum power for hovering UAV  $a_m$ . Furthermore, the associated sensing hovering energy is  $E_m^{hs} = P_m \times t_m^s$ , and the communication hovering energy is  $E_m^{hc} = P_m \times t_m^c$ , where  $t_m^s$  denotes the UAV's sensing hovering time for all users under its responsibility, and  $t_m^c$  denotes the communication hovering time with the DC.

The propulsion power during flight is given by  $P_m^f = \kappa_1 v_m^3(t) + \frac{\kappa_2}{v_m(t)} \times P_h$  [39], where  $\kappa_1$ ,  $\kappa_2$ , and  $P_h$  are constants determined by a particular type of the UAV. The flight time of the UAV, related to its flight path and speed (which will be calculated later), is initially denoted as  $t_m^f$ . Subsequently, the energy consumption of  $a_m$  during flight is given as

$$E_m^f = P_m^f \times t_m^f. \quad (8)$$

Thus, the total energy consumption of the UAV  $a_m$ , denoted as  $E_m^U$ , is given by  $E_m^U = E_m^{hs} + E_m^f + E_m^{hc}$ . Given that the on-board energy storage of each UAV is limited, denoted as  $E_{\max}$ , the total energy consumption  $E_m^U$  should adhere to the constraint as

$$E_m^U \leq E_{\max}. \quad (9)$$

### E. SENSING MODEL

We use the probabilistic path loss model [40] to characterize the air-to-ground communication between UAV  $a_m$  and user  $u_n$ . The Line-of-Sight (LoS) probability,  $\xi_{mn}^{\text{LoS}}$ , is given by  $\frac{1}{1+b_1e^{-b_2(\theta_{mn}^s-b_1)}}$ , where  $b_1$  and  $b_2$  are constants dependent on the environment. The elevation angle,  $\theta_{mn}^s$ , between UAV  $a_m$  and user  $u_n$  is defined as  $\frac{180}{\pi} \arctan(\frac{z_{C_n}-z_n}{d_{mn}})$ , where,  $z_{C_n}$  and  $z_n$  are the altitudes of the UAV at data CP and the user, respectively, and  $d_{mn} = \sqrt{(x_{C_n}-x_n)^2 + (y_{C_n}-y_n)^2 + (z_{C_n}-z_n)^2}$  represents their distance.

The Non-line-of-sight (NLoS) probability is then  $\xi_{mn}^{\text{NLoS}} = 1 - \xi_{mn}^{\text{LoS}}$ . The average channel power gain,  $\Omega_{mn}$ , is modeled as  $\rho_0 d_{mn}^{-2} [\xi_{mn}^{\text{LoS}} \mu^{\text{LoS}} + \xi_{mn}^{\text{NLoS}} \mu^{\text{NLoS}}]^2$ , where  $\rho_0$  is the channel power gain at 1 meter, and  $\mu^{\text{LoS}}$  and  $\mu^{\text{NLoS}}$  are attenuation factors.

Considering transmit power and channel gain, the UAV's signal-to-interference-to-noise ratio (SINR),  $\Psi_{mn}$ , for data collection from user  $u_n$  is defined as  $\frac{\Omega_{mn} P_m^s}{\sum_{u_i \in U_m, i \neq n} \Omega_{mi} P_m^s + \sigma^2}$ , where  $\sigma^2 = \mathcal{B} \delta_0$ , with  $\delta_0$  as the communication noise figure and  $\mathcal{B}$  as the system bandwidth.

The UAV's sensing data transmission rate,  $R_{mn}$ , is calculated using Shannon capacity formula:  $\mathcal{B} \log_2(1 + \Psi_{mn})$ . To ensure data quality, we set a threshold for each UAV's transmission rate,  $R_s^{\min}$ . Thus, we enforce the sensing data transmission constraint as

$$R_{mn} \geq R_s^{\min}. \quad (10)$$

We assume a minimum transmission rate (lower bound) to ensure that the sensing data is transmitted in a timely manner, adhering to the system's AoI requirements. This lower bound is chosen to avoid delays that could compromise the freshness and relevance of the data.

### F. COMMUNICATIONS MODEL

In addition to user sensing, each UAV communicates with the DC on different frequency bands, prioritizing on the signal-to-noise ratio (SNR) in the communication link. SINR is used in the sensing model to account for interference from other UAVs when collecting data from users. In contrast, SNR is used in the communication model for UAV-to-DC communication, where it's assumed that interference from other UAVs is negligible or managed effectively. This assumption can be achieved when UAVs operate on different frequency bands or interference mitigation techniques are used. Communication takes place when the UAV reaches a HP near the DC. The data transfer rate between UAV  $a_m$  at HP  $D_m$  and the DC is  $R_{m0} = \mathcal{B} \log_2(1 + \frac{\beta_0 P_m^c}{\sigma^2 d_{m0}^\rho})$ , where  $\rho$  is the path loss index, and  $d_{m0}$  is the distance between the UAV and the DC, given as  $d_{m0} = \sqrt{(x_{C_n}-X_0)^2 + (y_{C_n}-Y_0)^2 + (z_{C_n}-Z_0)^2}$ .

To ensure the quality of communication between each UAV and the DC, we establish a minimum transmission rate threshold,  $R_c^{\min}$ . Additionally, to keep the transmission rate within feasible limits, we introduce an upper bound,

$R_{\max}$ . Therefore, the data transmission constraint during the communication phase is defined as

$$R_c^{\min} \leq R_{m0} \leq R_{\max}. \quad (11)$$

In (10) and (11),  $R_s^{\min}$  and  $R_c^{\min}$  are set based on the minimum reliable distances  $d_1$  and  $d_2$  for sensing and communication, respectively. On the other hand,  $R_{\max}$  is chosen according to the UAV's maximum communication range  $r_0$ , as defined in (2).

## III. PROBLEM FORMULATION

### A. AGE OF INFORMATION (AOI)

The timeliness of sensing and communication significantly influences data validity. To quantify this, we use the concept of AoI, describing the freshness of data received by a DC, serving as a metric for system performance in this work.

Considering that the sensing data requires transmission to the DC, we define the AoI for each task based on its peak information age. Here,  $X_n^m(t)$  is the AoI for the sensing task of UAV  $a_m$  for user  $u_n$  at time  $t$ . When the sensing data is completely offloaded to the DC at time  $t^m$ , the AoI is given as  $X_n^m(t^m) = (t^m - t_n^m)^+$ , where  $t_n^m$  is the instant at which the sensing data of user  $u_n$  is sampled and  $(x)^+ = \max\{x, 0\}$ .

$X_n^m$  consists of five time components: UAV-to-user hovering time ( $t_{mn}^1$ ), UAV-to-remaining-users flight time ( $t_{mn}^2$ ), UAV-to-remaining-users hovering time ( $t_{mn}^3$ ), UAV-to-DC flight time ( $t_{mn}^4$ ), and UAV hovering time near the DC ( $t_{mn}^5$ ). Here, ( $t_{mn}^2$ ) and ( $t_{mn}^4$ ) are related to the path traveled by the UAV  $a_m$ , represented as  $\mathcal{R}_m = \{r_{m1}, r_{m2}, \dots, r_{mk_m}, r_{m(k_m+1)}\}$ , including all data CPs, i.e.,  $r_{mi} \in C_{pm} (\forall i \in \mathcal{K}_m = \{1, 2, \dots, k_m\})$ , and HP, i.e.,  $r_{m(k_m+1)} = (x_{D_m}, y_{D_m}, z_{D_m})$ . Thus, these flight times are given as

$$\sum_{u_n \in U_m} t_{mn}^2 = \sum_{i=1}^{k_m} \sum_{j=i}^{k_m-1} \frac{\|r_{m(j+1)} - r_{mj}\|_2}{v_m}, \quad (12)$$

$$\sum_{u_n \in U_m} t_{mn}^4 = \frac{\|r_{m(k_m+1)} - r_{mk_m}\|_2}{v_m} \quad (13)$$

where  $\|r_{m(j+1)} - r_{mj}\|_2$  denotes the UAV  $a_m$  travel distance from data CP  $r_{mj}$  to  $r_{m(j+1)}$ , with  $v_m$  as the UAV's flight speed.

Based on the sensing data transmission rate ( $R_{mn}$ ) from UAV  $a_m$  to user  $u_n$ , the total transmission time is  $T_n^m = \frac{W_n}{R_{mn}}$ , where  $W_n$  is the length of the packet generated at user  $u_n$ . Thus, the hover time ( $t_{mn}^1$ ) and ( $t_{mn}^3$ ) are

$$\sum_{u_n \in U_m} t_{mn}^1 = \sum_{j=1}^{k_m} T_j^m, \quad (14)$$

and

$$\sum_{u_n \in U_m} t_{mn}^3 = \sum_{i=1}^{k_m} \sum_{j=i+1}^{k_m} T_j^m, \quad (15)$$

respectively, where  $T_j^m$  represents the UAV  $a_m$  hovering time paired with  $r_{mj}$ , where  $j \in \mathcal{K}_m$ . This corresponds to the hover time dedicated to the respective user.

Similarly, the downlink transmission time between the UAV  $a_m$  and the DC is  $T_0^m = \frac{\sum_{u_n \in U_m} W_n}{R_{m0}}$ . In this regard, the hovering time near DC is given as

$$\sum_{u_n \in U_m} t_{mn}^5 = T_0^m. \quad (16)$$

The overall information age of the sensing tasks for UAV  $a_m$  is

$$X^m(R_m) = \sum_{u_n \in U_m} (t_{mn}^1 + t_{mn}^2 + t_{mn}^3 + t_{mn}^4 + t_{mn}^5). \quad (17)$$

Since all  $N$  users are sensed by  $M$  UAVs, the overall AoI of the entire system is expressed as

$$A_N = \sum_{m=1}^M X^m(R_m). \quad (18)$$

Thus, the problem can be formulated as

$$\begin{aligned} & \min_{\beta_{mi}, R_m, C_p, \mathcal{D}, \alpha_m^s, \alpha_m^c, v_m} A_N \\ & \text{s.t.} \\ & (3), (4), (5), (6), (7), (9), (10), (11) \end{aligned} \quad (19)$$

If a UAV hovers over each data CP and over each communication HP, meeting the respective distance criteria, it satisfies the anti-collision constraint (6). Thus, (6) can be replaced as

$$\begin{aligned} & \sqrt{(x_{C_{n_1}} - x_{C_{n_2}})^2 + (y_{C_{n_1}} - y_{C_{n_2}})^2 + (z_{C_{n_1}} - z_{C_{n_2}})^2} \\ & \geq D_{\min} \quad (n_1, n_2 \in U, n_1 \neq n_2) \end{aligned} \quad (20)$$

and

$$\begin{aligned} & \sqrt{(x_{D_{m_1}} - x_{D_{m_2}})^2 + (y_{D_{m_1}} - y_{D_{m_2}})^2 + (z_{D_{m_1}} - z_{D_{m_2}})^2} \\ & \geq D_{\min} \quad (m_1, m_2 \in A, m_1 \neq m_2) \end{aligned} \quad (21)$$

The constraints in (19) include limits on flight speed in (3), UAV range in (4) and (5), anti-collision measures in (6), hovering power in (7), overall energy in (9), sensing rates in (10), and communication rates in (11). However, constraints (4), (5), (16) and (17) are only associated with the optimization variables  $C_p$  and  $\mathcal{D}$ . Therefore, the optimization problem described in (19) is decomposed into two sub-problems:

- 1) *The hover coordinate optimization sub-problem* is established to generate the coordinates of the data CP ( $C_p$ ) and the communication HP coordinates ( $\mathcal{D}$ ).
- 2) *The path optimization sub-problem*, aimed at minimizing the information age, is formulated by optimizing the parameters  $\alpha_m^s$ ,  $\alpha_m^c$ ,  $v_m$ , and the task sequence of the UAV  $\Gamma_m = \{m_1, m_2, \dots, m_{k_m}\}$ , where  $m_i \in A$ .

## B. HOVER COORDINATE OPTIMIZATION

The hover coordinate optimization sub-problem involves determining the  $C_p$  and  $\mathcal{D}$ . Constraints for each user's data CP are given by (1), (4), and (16), while constraints for the communication HP are represented by (2), (5), and (17). In the optimization problem defined by (19), constraints (10) and (11) pertain to sensing and communication performances. These constraints can be relaxed to the minimum values of the distance between the data CP and the user, and the distance between the communication HP and the DC, respectively, as

$$\begin{aligned} & \sqrt{(x_{C_n} - x_{u_n})^2 + (y_{C_n} - y_{u_n})^2 + (z_{C_n} - z_{u_n})^2} \\ & \geq d_1, \quad n \in U \end{aligned} \quad (22)$$

and

$$\begin{aligned} & \sqrt{(x_{D_m} - X_0)^2 + (y_{D_m} - Y_0)^2 + (z_{D_m} - Z_0)^2} \\ & \geq d_2, \quad m \in A \end{aligned} \quad (23)$$

where  $d_1$  and  $d_2$  are the minimum sensing and communication distances calculated based on  $R_s^{\min}$  and  $R_c^{\min}$ , respectively.

The following describes the solutions for  $C_p$  and  $\mathcal{D}$ , respectively

$$\begin{aligned} & \min_{C_p} \sum_{n=1}^N \sqrt{(x_{C_n} - x_{u_n})^2 + (y_{C_n} - y_{u_n})^2 + (z_{C_n} - z_{u_n})^2} \\ & \text{s.t.} \\ & (1), (4), (16), (17), \end{aligned} \quad (24)$$

and

$$\begin{aligned} & \min_{\mathcal{D}} \sum_{m=1}^M \sqrt{(x_{D_m} - X_0)^2 + (y_{D_m} - Y_0)^2 + (z_{D_m} - Z_0)^2} \\ & \text{s.t.} \\ & (2), (5), (21), (22). \end{aligned} \quad (25)$$

## C. PATH OPTIMIZATION

After the analysis and solution in Section III-B, the set of hover coordinate  $C_p$  and  $\mathcal{D}$  can be obtained. Therefore, with only the knowledge of the task order of each UAV, we can obtain the indication factors for UAVs and tasks,  $\beta_{mi}$ , and the UAV flight paths  $R_m$ . Thus, the optimization problem described in (19) is simplified to the following optimization sub-problem to minimize AoI as

$$\begin{aligned} & \min_{\alpha_m^s, \alpha_m^c, v_m, T_m} A_N, \\ & \text{s.t.} \\ & (3), (7), (9), \sum_{i=1}^M k_m = N. \end{aligned} \quad (26)$$

where  $T_m$  represents the task sequence for all UAVs, and  $T_m = \{m_1, \dots, m_{k_m}\}$ , with  $m_i \in N$  denoting the order in which UAV  $a_m$  visits users, where  $m_i$  is the user index and  $k_m$  is the number of users assigned to UAV  $a_m$ .

#### IV. ALGORITHM DESIGN

PSO leverages group cooperation and information sharing to efficiently find optimal solutions, navigating both local and global optima. For minimizing information age in multi-UAV networks, we use VPSO and TVPSO, which are based on variable neighborhood search (VNS).

##### A. VARIABLE NEIGHBORHOOD PSO (VPSO)

PSO, inspired by natural entities like bird flocks [32], uses information exchange and random movement to find optimal solutions. In the context of the proposed VPSO, a particle represents a candidate solution within the UAV path planning problem. Each particle's position corresponds to a possible configuration of UAV tasks and resource allocations, and the swarm's collective behavior drives the search for the optimal configuration. Our VPSO algorithm enhances traditional PSO with several benefits for the optimization problem:

- 1) tailored coding and decoding (CODEC) strategies for UAV mission planning
- 2) fitness function based on minimizing information age
- 3) dynamic weight update strategy for enhanced optimization
- 4) population expansion using variable neighborhood search to mitigate local optima

##### 1) CODING AND DECODING (CODEC)

In the proposed VPSO, the swarm consists of  $S$  particles, each with a dimension  $D$  equal to the number of users in the system, denoted by  $N$ . The position of particle  $i$  in the  $l^{\text{th}}$  iteration is represented as  $x_i^l = (x_{i,1}^l, x_{i,2}^l, \dots, x_{i,D}^l)$  where each component  $x_{i,j}^l$  lies within the range  $x_{i,j}^l \in [0, hM)$ ,  $\forall j = 1, 2, \dots, D$ . Here,  $h$  is a positive integer known as the coding factor, chosen based on the system's number of UAVs and users.

The decoding strategy involves determining the user access order for each UAV in the system based on the position of each particle. First, the elements in  $x_i^l$  are sorted from smallest to largest, resulting in a new order denoted by  $j'$ . Subsequently, using the sorted values, the UAV responsible for accessing each user is decoded. For instance,  $x_{i,j}^l$  corresponds to the UAV number responsible for accessing user  $u_j$  as

$$\lambda_j = \left\lfloor \frac{x_{i,j}^l}{h} \right\rfloor + 1, \quad (27)$$

where, the operation  $\lfloor \cdot \rfloor$  denotes rounding down to the nearest integer. This process ensures that users assigned to the same UAV are grouped together. Subsequently, based on the sorted order  $j'$  of each element, the sequence in which each user  $j$  is accessed within the task queue of its corresponding UAV is determined. For instance, if both user  $u_1$  and user  $u_4$  are assigned to the task queue of UAV  $a_1$ , and  $u_1$  is sorted second, while  $u_4$  is sorted first, then the task order for UAV  $a_1$  is  $T_1 = \{4, 1\}$ .

##### 2) FITNESS FUNCTION

Utilizing the CODEC strategy in Section IV-A1, we derive the mission sequence for each UAV, denoted as  $T_m$ . Simultaneously, leveraging the DC point set attained from the hovering coordinate optimization sub-problem in Section III-B, denoted as  $C_p$ , and the communication HP set  $\mathcal{D}$ , we determine the flight path  $R_m$  for each UAV. Consequently, employing (18), we compute the overall information age of the system. Given that our optimization objective revolves around minimizing the information age, it directly serves as the fitness criterion denoted as  $F = A_N$ .

Utilizing this fitness calculation function, we compute the fitness value for each particle. For instance, in the  $l^{\text{th}}$  iteration, we identify the position with the lowest fitness among all positions of particle  $i$  from the previous  $l^{\text{th}}$  round, termed as the individual optimal position of the particle. This is represented as  $x_i^b$ , where  $i = 1, 2, \dots, S$ , and its corresponding fitness is denoted as  $F_i^b$ , with  $i = 1, 2, \dots, S$ . Furthermore, the position with the minimum fitness across all particles is termed as the optimal position of the group, denoted as  $x_{gb}$ , and its corresponding global minimum fitness is denoted as  $F_{gb}$ .

##### 3) DYNAMIC WEIGHT UPDATE STRATEGY

In the PSO algorithm, each particle's position is updated using its current position and respective update speed. Here,  $u_i^l$  represents the update speed of particle  $i$  in the  $l^{\text{th}}$  round. Consequently, the position of particle  $i$  in the next round is calculated as

$$x_i^{l+1} = x_i^l + u_i^{l+1}. \quad (28)$$

The updating of position of individual particles is influenced by both the individual's optimal position and the group's optimal position. This updating process comprises three components: the memory term, individual cognitive term, and group cognitive term. The memory term signifies the current velocity, influenced by the magnitude and direction of the previous velocity. The individual cognitive term reflects particles' inclination to explore their individual optimal solutions within the solution space. On the other hand, the group cognitive term signifies particles' inclination to explore the optimal solution within the entire neighborhood, showcasing collaboration and knowledge sharing among particles. The update rate of particle  $i$  in the  $l+1$  round is given as

$$u_i^{(l+1)} = \omega^l \times u_i^l + c_1 \eta_1 \times (x_i^b - x_i^l) + c_2 \eta_2 \times (x_{gb} - x_i^l), \quad (29)$$

where  $c_1$  and  $c_2$  represent the individual and social learning factors, respectively, and are typically set to 2. The individual learning factor encourages a particle to move towards its own best-known position, while the social learning factor guides it towards the best-known position found by the swarm. Meanwhile,  $\eta_1$  and  $\eta_2$  are random numbers drawn from the

interval  $[0, 1]$ .  $\omega^l$  denotes the inertia weight factor, with values typically constrained within  $[0, 1]$ . A larger  $\omega^l$  enhances global search capabilities, allowing for exploration of new candidate solutions within the solution space. Conversely, a smaller  $\omega^l$  improves local search abilities, facilitating algorithm convergence. Thus, the dynamic weight update strategy with non-linearly decreasing dynamic weights in VPSO can be employed as

$$\omega^l = \omega_2 \times \left( \frac{\omega_1}{\omega_2} \right)^{\frac{1}{1+\frac{l}{L}}}, \quad (30)$$

where  $\omega_1$  represents the initial weight,  $\omega_2$  represents the final weight, and  $\omega_1 > \omega_2$ .  $L$  represents the total number of iterations.

#### 4) VARIABLE NEIGHBORHOOD SEARCH (VNS) EXTENSION

VPSO utilizes three neighborhood structures to discover improved solutions, with each neighborhood containing a set of candidate particles, denoted as  $S_V$ . During each iteration, the particle position with the lowest fitness among the  $S$  particles in the original search space is chosen as the source position. Subsequently, candidate particles are generated in the three neighborhoods based on specific perturbation rules determined by the source position. For instance, in the  $l^{\text{th}}$  iteration,  $x_{b_l}$  represents the source position, and the generation rules for the other candidate particles are outlined as

- 1) Randomly select two integers  $i$  and  $j$  from the interval  $[1, N]$ , then swap the positions of the  $i^{\text{th}}$  and  $j^{\text{th}}$  elements in  $x_{b_l}$ . Repeat this process  $S_V$  times to generate the set of candidate particles in neighborhood 1 denoted as  $z_{q_l}$ , where  $q = 1, 2, \dots, S_V$ .
- 2) Generate four random integers within the interval  $[1, N]$ :  $i_1, i_2, j_1, \text{ and } j_2$ . Then, perform the following exchanges: swap the  $i_1^{\text{th}}$  element with the  $j_1^{\text{th}}$  element, and swap the  $i_2^{\text{th}}$  element with the  $j_2^{\text{th}}$  element in  $x_{b_l}$ . Repeat this process  $S_V$  times to obtain a set of candidate particles in neighborhood 2, denoted as  $e_{q_l}^l$ , where  $q$  ranges from 1 to  $S_V$ .
- 3) Generate six random integers within the interval  $[1, N]$ :  $i_1, i_2, i_3, j_1, j_2, \text{ and } j_3$ . Then, perform the following swaps: exchange the  $i_1^{\text{th}}$  element with the first  $j_1^{\text{th}}$  element, the  $i_2^{\text{th}}$  element with the first  $j_2^{\text{th}}$  element, and the first  $i_3^{\text{th}}$  element with the first  $j_3^{\text{th}}$  element in  $x_{b_l}$ . Repeat this process  $S_V$  times to obtain a set of candidate particles in neighborhood 3, denoted as  $h_{q_l}$ , where  $q$  ranges from 1 to  $S_V$ .
- 4) After generating candidate particles for each neighborhood, a total of  $3 S_V$  candidate particles are obtained. The fitness of each candidate particle is individually calculated using the fitness function defined in (27). If a particle's fitness is lower than the global minimum fitness,  $F_{gb}$ , it is updated to the new global optimal position, and the global minimum fitness is updated to the fitness of that particle.

---

#### Algorithm 1 VPSO Algorithm

---

**Input:**  $C_p, \mathcal{D}, \alpha_m^s, \alpha_m^c$ , and  $v_m$ .

**Output:**  $F_{gb}, T_m^b$ , and average energy consumption of UAVs.

---

- 1: Initialize the position and velocity of all  $S$  particles,  $F_i^b$  and  $F_{gb}$ ;
  - 2: Calculate the initial fitness values of  $S$  particles, update  $F_i^b$  and  $F_{gb}$ , determine  $x_i^b$  and  $x_{gb}$ ;
  - 3: **for**  $l = 1, 2, \dots, L$  **do**
  - 4:   Calculate the update velocity of each particle in this round according to (29);
  - 5:   Follow (28) to update the position of each particle.
  - 6:   According to the decoding strategy described in Section IV-A1, obtain the UAV task arrangement corresponding to each particle;
  - 7:   Calculate the fitness of each particle based on the decoded UAV task arrangement;
  - 8:   Update  $F_i^b, F_{gb}, x_i^b$ , and  $x_{gb}$  based on the fitness of the particles, and determine the source position of the variable neighborhood  $x_{b_l}^l$ ;
  - 9:   Decode the UAV task arrangement obtained from  $x_{gb}$  update to  $T_m^b$ ;
  - 10:   **for**  $k = 1, 2, 3$  **do**
  - 11:     **if**  $k = 1$  **then**
  - 12:       Generate  $z_q^l$  according to Rule (4) in Section IV-A4 and calculate fitness;
  - 13:     **else if**  $k = 2$  **then**
  - 14:       Generate  $e_q^l$  according to Rule (4) in Section IV-A4 and calculate fitness;
  - 15:     **else if**  $k = 3$  **then**
  - 16:       Generate  $h_q^l$  according to Rule (4) in Section IV-A4 and calculate fitness;
  - 17:     **end if**
  - 18:     Update fitness less than  $F_{gb}$  to the new  $F_{gb}$ , and update the corresponding particle position to  $x_{gb}$ ;
  - 19:   **end for**
  - 20: **end for**
  - 21: Compute the energy consumption of each UAV based on (8), and calculate the average energy consumption  $\frac{1}{M} \sum_{m=1}^M E_U^m$ .
- 

The specific details of the algorithm implementation are provided in Algorithm 1.

#### B. TWIN VARIABLE PSO (TVPSO)

The UAV's velocity and parameters must be optimized considering the AoI from task planning, as they are interdependent. This paper proposes a dual PSO algorithm based on VNS, consisting of an external swarm optimizing UAV velocity and parameters and an internal swarm optimizing UAV paths. The nested dual swarm structure allows alternating optimization of these coupled items, while the variable neighborhood methods expand the search space, avoiding local optima and achieving global optimization.

The following sections detail the design of the external PSO algorithm.

#### 1) PARTICLE POSITION DESIGN BASED ON PARAMETER FUSION

In the external particle swarm, the number of particles is set to  $S_T$ . Since the optimization of the external particle swarm includes three components, i.e., UAV speed, sensing power allocation parameters, and communication power allocation parameters, the dimension  $D_T$  of the particles is three times the number of UAVs  $M$  in the system, i.e.,  $D_T = 3M$ . The maximum number of iterations for the external particle swarm is denoted as  $G$ .

The position of particle  $j$  in the  $g$ -th iteration is given as

$$y_j^g = (y_{j,1}^g, y_{j,2}^g, \dots, y_{j,3D}^g). \quad (31)$$

- The first  $M$  elements ( $y_{j,1}^g, y_{j,2}^g, \dots, y_{j,M}^g$ ) represent the flight speed of each UAV,  $v_m$ , with a range of  $[v_{\min}, v_{\max}]$ .
- The middle  $M$  elements ( $y_{j,M+1}^g, y_{j,M+2}^g, \dots, y_{j,2M}^g$ ) represent the sensing power allocation parameters of each UAV,  $\alpha_m^s$ , with a range of  $[0.1, 0.9]$ .
- The last  $M$  elements ( $y_{j,2M+1}^g, y_{j,2M+2}^g, \dots, y_{j,3M}^g$ ) represent the communication power allocation parameters of each UAV,  $\alpha_m^c$ , also with a range of  $[0.1, 0.9]$ .

#### 2) HYBRID FITNESS CALCULATION FUNCTION

The fitness calculation of each particle in TVPSO is related to the particle's position and the optimization results of each particle in the VPSO algorithm. Taking the  $g^{\text{th}}$  iteration as an example, the position  $y_i^g$  of the  $i^{\text{th}}$  particle is used as input for the VPSO algorithm. After  $L$  iterations in VPSO, the optimal flight path  $R_m$  for each UAV can be obtained. In the optimization of the VPSO algorithm, the focus is on minimizing the information age for UAV path optimization. Therefore, the fitness function value is the minimum information age of the system after optimization. However, in the global optimization problem based on minimizing the information age proposed in (19). There are also constraints on the energy consumption of UAVs. Therefore, to minimize the total energy consumption of each UAV in the final optimization solution as much as possible, the TVPSO algorithm uses a hybrid fitness calculation function based on weights as

$$F_T = \phi \sum_{m=1}^M E_m^U + (1 - \phi) \sum_{m=1}^M X^m. \quad (32)$$

where  $\phi$  is the blending ratio factor, representing the weight of energy consideration in the fitness function calculation.

Based on this fitness calculation function, the fitness of each particle can be computed. Taking the  $g^{\text{th}}$  iteration as an example, the position corresponding to the minimum fitness among all positions of particle  $j$  in the previous  $g$  iterations is termed as the individual best position of the particle, denoted as  $y_j^b$ , with the corresponding fitness  $F_{T_j}^b$ . The position with

the minimum fitness among all particles is termed as the global best position, denoted as  $y_{gb}$ , with the corresponding global minimum fitness  $F_{T_{gb}}$ .

#### 3) PARTICLE UPDATE BASED ON DYNAMIC WEIGHTS

Similar to the particle positions, the particle update velocities in TVPSO correspond to increments in UAV velocity, sensing power allocation, and communication power allocation parameters. Let  $w_j^g$  denotes the update velocity of particle  $j$  at the  $g^{\text{th}}$  iteration. Then, the position of particle  $j$  in the next iteration is given by

$$y_j^{g+1} = y_j^g + w_j^{g+1}. \quad (33)$$

The position of particle  $j$  is updated at the rate of  $g+1$  as

$$w_j^{g+1} = \omega_T^g \times w_j^g + c_3 \eta_3 \times (y_j^b - y_j^g) + c_4 \eta_4 \times (y_{gb} - y_j^g). \quad (34)$$

where  $c_3$  and  $c_4$  represent the individual and social learning factors, typically set to 2.  $\eta_3$  and  $\eta_4$  are random numbers between 0 and 1.  $\omega_T^g$  denotes the inertia weight factor, which ranges from 0 to 1 and is usually assigned a fixed value. A larger  $\omega_T^g$  indicates stronger global search capability, exploring more new candidate solutions in the solution space, while a smaller  $\omega_T^g$  enhances local search capability, accelerating algorithm convergence. Therefore, in TVPSO, a non-linearly decreasing dynamic weight update strategy is employed as

$$\omega_T^g = \omega_4 \times \left( \frac{\omega_3}{\omega_4} \right)^{\frac{1}{1 + \frac{10g}{G}}}. \quad (35)$$

where  $\omega_3$  and  $\omega_4$  represent the initial and final weights, respectively, with  $\omega_3$  being greater than  $\omega_4$  and  $G$  represents the total number of iterations.

#### 4) VARIABLE NEIGHBORHOOD SEARCH EXTENSION IN TVPSO

TVPSO incorporates three neighborhood structures, each with  $S_{TV}$  candidate particles. In each iteration, the position of the particle with the lowest fitness among the  $S_T$  particles in the original search space serves as the source position. Subsequently, candidate particles for the three neighborhoods are generated based on this source position using specific disturbance rules. For instance, in the  $g^{\text{th}}$  iteration,  $y_b^g$  represents the source position. The generation rules for other candidate particles are as follows

- 1) To exchange the velocities of any two UAVs, randomly select two integers,  $i$  and  $j$ , within the specified interval  $[1, M]$ . Swap the positions of the  $i^{\text{th}}$  and  $j^{\text{th}}$  elements in  $y_b^g$  to generate a candidate particle. Repeat this process  $S_{TV}$  times to create a set of candidate particles in neighborhood 1.
- 2) To exchange the sensing power allocation parameters of any two UAVs, randomly select two integers  $i$  and  $j$  within the specified interval  $[M+1, 2M]$ . Swap the positions of the  $i^{\text{th}}$  and  $j^{\text{th}}$  elements in  $y_b^g$  to obtain

TABLE 1. Simulation parameters.

Parameter	Value
Urban environment	$b_1, b_2, \mu_{LoS}, \mu_{NLoS}$ [40]
Simulation area (m)	$1000 \times 1000 \times 30$
Number of UAVs	5
Number of users	30
Bandwidth (bits/sec)	$10^6$
Size of sensing data (bits)	$2 \times 10^7$
UAV flight speed range (m/s)	[30,50]
UAV propulsion power (W)	[5,10]
UAV hovering power (W)	5
DC coordinates (m)	(500,500,20)
Distance constraint from CP to user (m)	[30,40]
Distance constraint from HP to DC (m)	[10,15]
Minimum distance between UAVs (m)	5

a candidate particle. Repeat this process  $S_{TV}$  times to generate a set of candidate particles in neighborhood 2.

- 3) To exchange the communication power allocation parameters of any two UAVs, randomly generate two integers  $i$  and  $j$  within the specified interval  $[2M + 1, 3M]$ . Swap the positions of the  $i$ -th and  $j$ -th elements in  $y_b^g$  to obtain a candidate particle. Repeat this process  $S_{TV}$  times to derive a set of candidate particles in neighborhood 3.

Thus, a total of  $3S_V$  candidate particles are obtained. Calculate each particle's fitness using the fitness function in (32). If a particle's fitness is less than the global minimum fitness  $F_{T_{gb}}$ , update the global best position and set the global minimum fitness to this particle's fitness.

In the proposed VPSO and TVPSO algorithms, the initial values of particles (i.e., potential solutions) are randomly generated within predefined bounds. This approach is common in PSO algorithms to promote diversity in the population and prevents premature convergence [41]. Each particle's position and velocity are randomly set within the search space, ensuring broad exploration while boundary constraints keep particles within feasible limits. This balances exploration and exploitation, aiding effective convergence.

## V. NUMERICAL RESULTS AND DISCUSSION

In this section, we evaluate the impact of various design parameters on both the AoI and energy consumption within a multi-UAV, multi-user scenario. We set up the simulation model in the MATLAB environment. Unless otherwise stated, simulation parameters are presented in Table 1.

### A. IMPACT OF DIFFERENT DESIGN PARAMETERS ON THE INFORMATION AGE AND ENERGY CONSUMPTION USING VPSO ALGORITHM

Fig. 3-6 in this subsection investigates the differences in optimization results of the optimal information age under

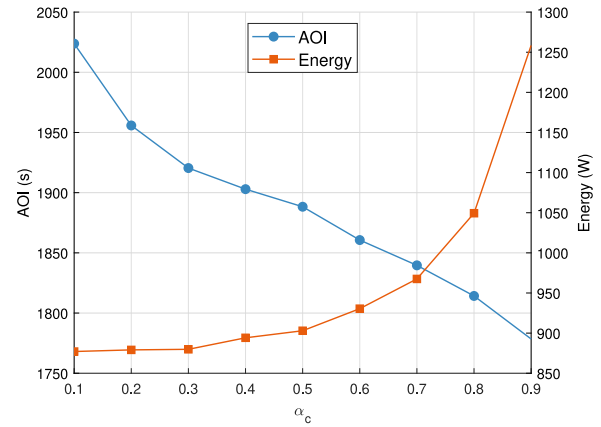


FIGURE 3. Impact of communication power ratio on information age and energy consumption.

communication power ratio  $\alpha_c$ , sensing power ratio  $\alpha_s$ , and number of UAVs and users. Each simulation yields results based on the VPSO algorithm under the same hover coordinate optimization. The VPSO algorithm's maximum iteration count is set to 200, with individual learning factor  $c_1$  and social learning factor  $c_2$  both set to 2. Initial weight  $\omega_1$  and final weight  $\omega_2$  are set to 0.4 and 0.9, respectively. The number of particles  $S$  is set to 50, with  $S_V$ , the number of candidate particles in each neighborhood, set to 10. Particle dimension  $D$  equals the number of users.

Fig. 3 illustrates the impact of varying the communication power ratio ( $\alpha_c$ ) on the minimum information age and average energy consumption of UAVs in a multi-UAV-assisted network. The simulations are conducted with fixed parameters:  $M = 5$  (number of UAVs),  $N = 30$  (number of users),  $\alpha_s$  (sensing power ratio), and  $v = 40$  km/h (UAV speed), while  $\alpha_c$  ranges from 0.1 to 0.9. Specifically, the results in Fig. 3 are obtained by solving the optimization problem in (19) using the framework in Algorithm 1. As  $\alpha_c$  increases, the minimum AoI decreases, reflecting fresher data due to faster communication. However, this comes at the cost of higher energy consumption, as increased communication power requires more energy for data transmission. The results highlight a trade-off: while higher  $\alpha_c$  improves data timeliness, it also raises energy expenditure for the UAVs. Thus, in a trade-off scenario,  $\alpha_c = 0.6$  might be considered optimal, as it provides a reasonable reduction in AoI while keeping energy consumption at a manageable level, avoiding the extremes of either metric.

Fig. 4 presents the results of simulations conducted to examine the impact of varying the sensing power ratio ( $\alpha_s$ ) on the minimum information age and the average energy consumption of UAVs. The simulations are conducted with fixed parameters:  $M = 5$  (number of UAVs),  $N = 30$  (number of users),  $\alpha_c$  (communication power ratio), and  $v = 40$  (UAV speed), while  $\alpha_s$  ranges from 0.1 to 0.9. These results rely on the UAV energy model in (8) and the communication model in (11), which together define

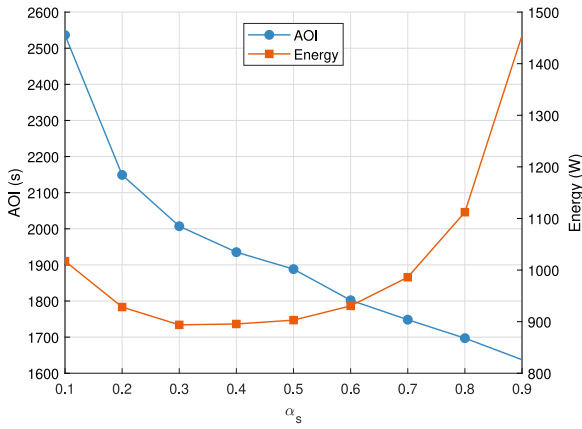


FIGURE 4. Impact of sensing power ratio on information age and energy consumption.

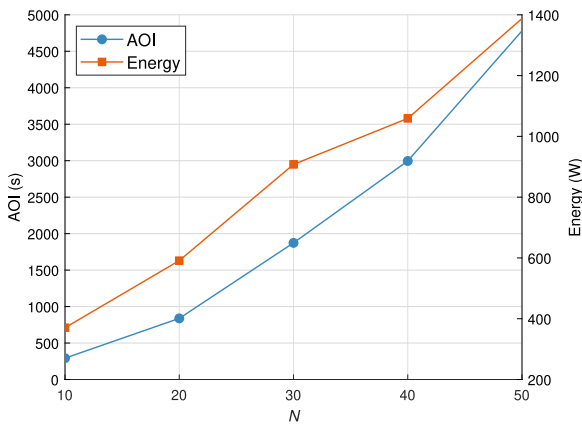


FIGURE 5. Impact of number of users on information age and energy consumption.

how energy consumption and transmission rates are managed within the proposed optimization scheme in Algorithm 1. As  $\alpha_s$  increases, the minimum information age decreases, indicating that UAVs can gather and update information more quickly. Concurrently, the average energy consumption of the UAVs first decreases and then increases. For an optimal trade-off between AoI and energy consumption in Fig. 4,  $\alpha_s = 0.5$  is a strong candidate. It provides a balance that avoids the extremes of high energy consumption or high AoI, making it suitable for scenarios where both metrics need to be optimized.

Fig. 5 illustrates the impact of varying the number of users ( $N$ ) on the minimum information age and the average energy consumption of UAVs in a data collection mission. The parameters are fixed with communication power ratio ( $\alpha_c$ ) set at 0.5, sensing power ratio ( $\alpha_s$ ) at 0.5, UAV speed ( $v$ ) at 40 km/h, and the number of UAVs ( $M$ ) at 5. As the number of users increases from 10 to 50, both the minimum information age (AoI) and the average energy consumption of the UAVs rise. This is because more users lead to greater resource contention, causing UAVs to spend more time and energy completing their tasks. Conversely, with fewer users,

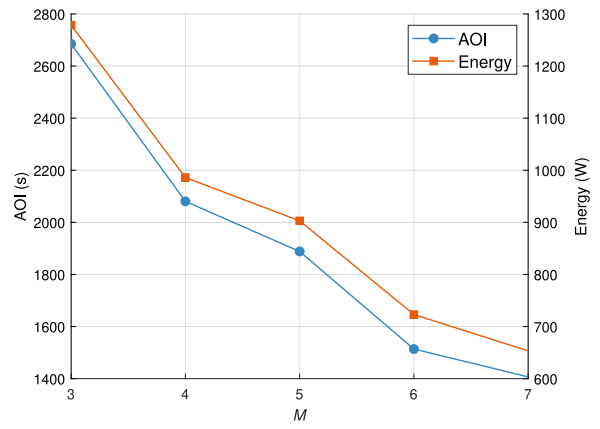


FIGURE 6. Impact of number of UAVs on information age and energy consumption.

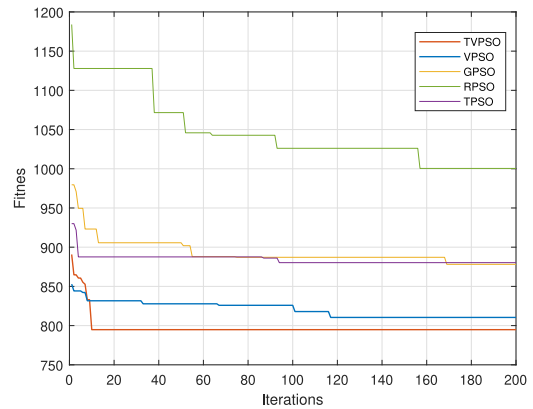


FIGURE 7. Fitness convergence of various optimization algorithms.

resource utilization is more efficient, resulting in better overall performance.

Fig. 6 illustrates the minimum information age and corresponding average UAV energy consumption as the number of UAVs ranges from 3 to 7. It's noticeable that with an increase in the number of UAVs, both the information age and the average energy consumption decrease. The trend occurs because there are more resources available for data collection and communication tasks. This enables a better distribution of tasks among the UAVs, reducing congestion and overall workload.

### B. IMPACT OF DIFFERENT OPTIMIZATION ALGORITHMS ON THE INFORMATION AGE AND ENERGY CONSUMPTION

Fig. 7 shows the convergence behavior of five algorithms over 200 iterations: GPSO, TVPSO, RPSO, VPSO, and TPSO. The results indicate that TVPSO achieves the best fitness convergence, outperforming the other PSO-based algorithms. This superior performance is due to TVPSO's time-varying nature, which expands the search space and helps avoid local optima. In contrast, RPSO demonstrates the weakest convergence, highlighting the inefficiency of random parameter optimization. GPSO and TPSO show moderate performance, better than RPSO but not as effective

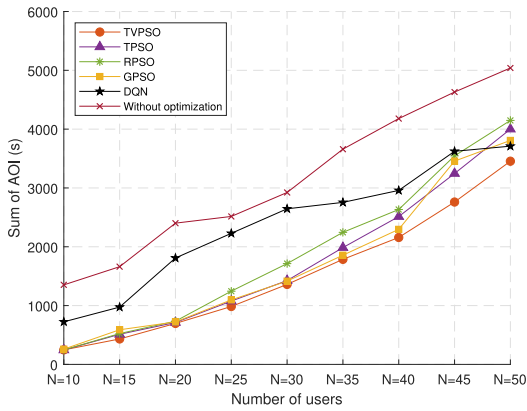


**FIGURE 8.** Impact of various optimization algorithms on information age for different numbers of users.

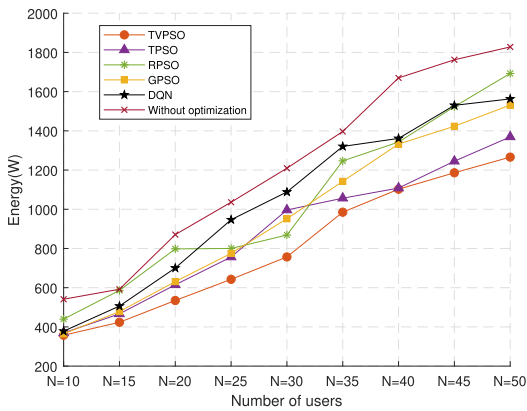


**FIGURE 9.** Impact of various optimization algorithms on the energy consumption for different numbers of users.

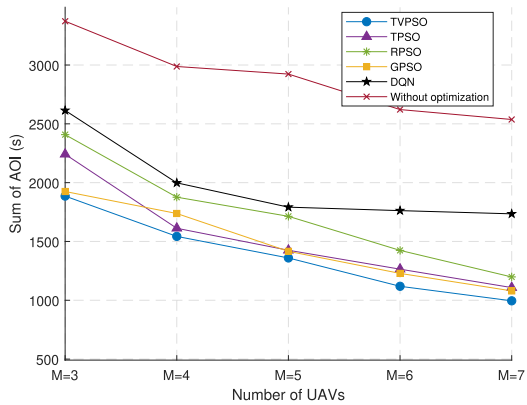


**FIGURE 10.** Impact of various optimization algorithms on information age for different numbers of UAVs.

as TVPSO and VPSO. TVPSO also surpasses VPSO due to its dual-swarm structure, which enhances search space exploration and solution quality, justifying its increased computational demands.

Figs. 8-11 in this subsection, present a comparative analysis of the performances of TVPSO against three PSO-based algorithms: Grey Wolf PSO (GPSO), Traditional PSO (TPSO), and Random Parameter Optimization with

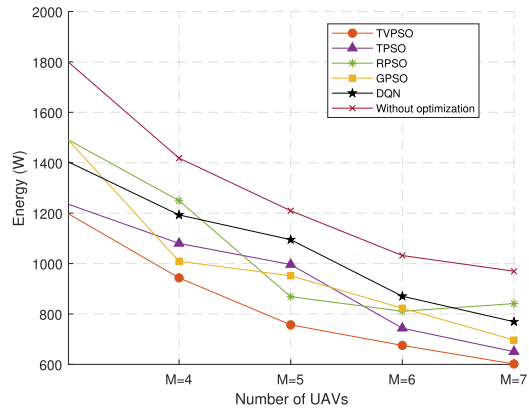


**FIGURE 11.** Impact of various optimization algorithms on the energy consumption for different numbers of UAVs.

PSO (RPSO), as well as DQN, both with and without optimization. The maximum iteration count for TVPSO and the three baseline algorithms is set to 200. In the particle swarm algorithm, the number of particles is set to 50, and both individual and social learning factors are set to 2. The initial weight and final weight, which decrease non-linearly, are set to 0.9 and 0.4, respectively. In the Grey Wolf algorithm, the pack size is set to 50, and the convergence factor during position updates linearly decreases from 2 to 0 over the iterations. All four algorithms are simulated under the same system model and hover coordinate optimization results.

Fig. 8 and 9 show how the total sum of information age and maximum energy consumption vary across six approaches, with a constant number of UAVs at 5 and users ranging from 10 to 50. In Fig. 8, the total sum of information age increases as the number of users rises for all four PSO-based algorithms, as well as for the DQN-based approach, both with and without optimization. TVPSO consistently achieves the lowest total sum of information age, outperforming the other PSO-based and DQN-based methods. The performance ranking from best to worst is as follows: GPSO, TPSO, RPSO, DQN with optimization, and DQN without optimization.

Fig. 9 shows that maximum energy consumption per UAV rises as the number of users increases for all approaches due to the higher number of access tasks per UAV. TVPSO consistently exhibits lower maximum energy consumption compared to the other approaches, indicating superior performance. The other approaches display some fluctuations in optimization results.

Fig. 10 and 11 show the variation in the total sum of information age and maximum energy consumption across six approaches, with a fixed number of users at 30 and the number of UAVs ranging from 3 to 7. In Fig. 10, the total sum of information age decreases as the number of UAVs increases for all approaches. TVPSO consistently achieves a lower total sum of information age compared to the other five approaches, demonstrating superior performance.

Among the other methods, the DQN approach without optimization performs the worst, while GPSO and TPSO show fluctuations at  $M = 3$  and  $M = 4$ , followed by consistent performance up to  $M = 7$ .

Fig. 11 shows that the maximum energy consumption per UAV decreases as the number of UAVs increases for all six approaches, due to the reduced number of access tasks per UAV. TVPSO consistently exhibits lower maximum energy consumption compared to the other approaches, demonstrating superior performance. The results for the other three PSO-based algorithms display some fluctuations.

## VI. CONCLUSION

In this paper, we have investigated and addressed the optimization of resource allocation and flight trajectories for multiple UAVs within a multi-UAV network serving multiple ground users, with the goal of minimizing the AoI. We have formulated the problem by jointly optimizing power allocation, bandwidth distribution, and UAV trajectories to achieve the lowest possible AoI for the collected data. To solve this complex optimization problem, we have proposed two algorithmic frameworks based on swarm optimization: VPSO and TVPSO. Numerical results have demonstrated that TVPSO consistently outperforms other algorithms, including GPSO, traditional PSO, RPSO, and a non-PSO-based method (DQN-based approach), in both AoI and energy consumption performances. Furthermore, our findings reveal that the optimal AoI is significantly influenced by factors such as sensing and communication power ratios, as well as the number of UAVs and users in the network. These insights provide valuable guidelines for designing and optimizing multi-UAV systems in practical applications.

## REFERENCES

- [1] P. Pace, G. Aloï, R. Gravina, G. Caliciuri, G. Fortino, and A. Liotta, "An edge-based architecture to support efficient applications for healthcare industry 4.0," *IEEE Trans. Ind. Informat.*, vol. 15, no. 1, pp. 481–489, Jan. 2019.
- [2] Q. Cui, J. Zhang, X. Zhang, K.-C. Chen, X. Tao, and P. Zhang, "Online anticipatory proactive network association in mobile edge computing for IoT," *IEEE Trans. Wireless Commun.*, vol. 19, no. 7, pp. 4519–4534, Jul. 2020.
- [3] M. A. Hoque, M. Hossain, S. Noor, S. M. R. Islam, and R. Hasan, "IoTaaS: Drone-based Internet of Things as a service framework for smart cities," *IEEE Internet Things J.*, vol. 9, no. 14, pp. 12425–12439, Jul. 2022.
- [4] G. Li et al., "Energy efficient data collection in large-scale Internet of Things via computation offloading," *IEEE Internet Things J.*, vol. 6, no. 3, pp. 4176–4187, Jun. 2019.
- [5] M. Samir, S. Sharafeddine, C. M. Assi, T. M. Nguyen, and A. Ghayeb, "UAV trajectory planning for data collection from time-constrained IoT devices," *IEEE Trans. Wireless Commun.*, vol. 19, no. 1, pp. 34–46, Jan. 2020.
- [6] H. Shakhatareh et al., "Unmanned Aerial Vehicles (UAVs): A survey on civil applications and key research challenges," *IEEE Access*, vol. 7, pp. 48572–48634, 2019.
- [7] S. A. H. Mohsan, M. A. Khan, F. Noor, I. Ullah, and M. H. Alsharif, "Towards the unmanned aerial vehicles (UAVs): A comprehensive review," *Drones*, vol. 6, no. 6, p. 147, 2022.
- [8] S. Hu, W. Ni, X. Wang, A. Jamalipour, and D. Ta, "Joint optimization of trajectory, propulsion, and thrust powers for covert UAV-on-UAV video tracking and surveillance," *IEEE Trans. Inf. Forensics Security*, vol. 16, pp. 1959–1972, 2021.
- [9] S. Hu, Q. Wu, and X. Wang, "Energy management and trajectory optimization for UAV-enabled legitimate monitoring systems," *IEEE Trans. Wireless Commun.*, vol. 20, no. 1, pp. 142–155, Jan. 2021.
- [10] T. Keawboontan and M. Thammawichai, "Toward real-time UAV multi-target tracking using joint detection and tracking," *IEEE Access*, vol. 11, pp. 65238–65254, 2023.
- [11] D. Tondas, K. Kazmierski, and J. Kaplon, "Real-time and near real-time displacement monitoring with GNSS observations in the mining activity areas," *IEEE J. Sel. Topics Appl. Earth Observ.*, vol. 16, pp. 5963–5972, Jun. 2023. [Online]. Available: <https://ieeexplore.ieee.org/document/10168211>
- [12] Y. Wu, Y. Sui, and G. Wang, "Vision-based real-time aerial object localization and tracking for UAV sensing system," *IEEE Access*, vol. 5, pp. 23969–23978, 2017.
- [13] J. A. Zhang et al., "An overview of signal processing techniques for joint communication and radar sensing," *IEEE J. Sel. Topics Signal Process.*, vol. 15, no. 6, pp. 1295–1315, Nov. 2021.
- [14] S. Lu, F. Liu, and L. Hanzo, "The degrees-of-freedom in monostatic ISAC channels: NLoS exploitation vs. reduction," *IEEE Trans. Veh. Technol.*, vol. 72, no. 2, pp. 2643–2648, Feb. 2023.
- [15] Z. Du et al., "Integrated sensing and communications for V2I networks: Dynamic predictive beamforming for extended vehicle targets," *IEEE Trans. Wireless Commun.*, vol. 22, no. 6, pp. 3612–3627, Jun. 2023.
- [16] K. Meng, Q. Wu, S. Ma, W. Chen, and T. Q. S. Quek, "UAV trajectory and beamforming optimization for integrated periodic sensing and communication," *IEEE Wireless Commun. Lett.*, vol. 11, no. 6, pp. 1211–1215, Jun. 2022.
- [17] Z. Lyu, G. Zhu, and J. Xu, "Joint maneuver and beamforming design for UAV-enabled integrated sensing and communication," *IEEE Trans. Wireless Commun.*, vol. 22, no. 4, pp. 2424–2440, Apr. 2023.
- [18] K. Meng, Q. Wu, S. Ma, W. Chen, K. Wang, and J. Li, "Throughput maximization for UAV-enabled integrated periodic sensing and communication," *IEEE Trans. Wireless Commun.*, vol. 22, no. 1, pp. 671–687, Jan. 2023.
- [19] K. Meng et al., "UAV-enabled integrated sensing and communication: Opportunities and challenges," *IEEE Wireless Commun.*, vol. 31, no. 2, pp. 97–104, Apr. 2024.
- [20] S. Kaul, R. Yates, and M. Gruteser, "Real-time status: How often should one update?" in *Proc. IEEE INFOCOM*, 2012, pp. 2731–2735.
- [21] C. Xu, H. H. Yang, X. Wang, and T. Q. S. Quek, "Optimizing information freshness in computing-enabled IoT networks," *IEEE Internet Things J.*, vol. 7, no. 2, pp. 971–985, Feb. 2020.
- [22] S. Zhang, H. Zhang, Z. Han, H. V. Poor, and L. Song, "Age of information in a cellular Internet of UAVs: Sensing and communication trade-off design," *IEEE Trans. Wireless Commun.*, vol. 19, no. 10, pp. 6578–6592, Oct. 2020.
- [23] H. Hu, K. Xiong, G. Qu, Q. Ni, P. Fan, and K. B. Letaief, "AoI-minimal trajectory planning and data collection in UAV-assisted wireless powered IoT networks," *IEEE Internet Things J.*, vol. 8, no. 2, pp. 1211–1223, Jan. 2021.
- [24] J. Liu, P. Tong, X. Wang, B. Bai, and H. Dai, "UAV-aided data collection for information freshness in wireless sensor networks," *IEEE Trans. Wireless Commun.*, vol. 20, no. 4, pp. 2368–2382, Apr. 2021.
- [25] T. Liang et al., "Age of information based scheduling for UAV aided localization and communication," *IEEE Trans. Wireless Commun.*, vol. 23, no. 5, pp. 4610–4626, May 2024.
- [26] W. Jiang, B. Ai, C. Shen, M. Li, and X. Shen, "Age-of-information minimization for UAV-based multi-view sensing and communication," *IEEE Trans. Veh. Technol.*, vol. 73, no. 1, pp. 1100–1114, Jan. 2024.
- [27] M. Samir, C. Assi, S. Sharafeddine, D. Ebrahimi, and A. Ghayeb, "Age of information aware trajectory planning of UAVs in intelligent transportation systems: A deep learning approach," *IEEE Trans. Veh. Technol.*, vol. 69, no. 11, pp. 12382–12395, Nov. 2020.
- [28] O. Rahimi and A. Sharafeddine, "Minimizing age of information in multi-UAV-assisted IoT networks: A graph theoretical approach," *Wireless Netw.*, vol. 30, no. 1, pp. 533–555, 2024.
- [29] Y. Pan, Y. Yang, and W. Li, "A deep learning trained by genetic algorithm to improve the efficiency of path planning for data collection with multi-UAV," *IEEE Access*, vol. 9, pp. 7994–8005, 2021.
- [30] Z. Yu, Z. Si, X. Li, D. Wang, and H. Song, "A novel hybrid particle swarm optimization algorithm for path planning of UAVs," *IEEE Internet Things J.*, vol. 9, no. 22, pp. 22547–22558, Nov. 2022.

- [31] Y. Jia et al., "The UAV path coverage algorithm based on the greedy strategy and ant colony optimization," *Electronics*, vol. 11, no. 17, p. 2667, 2022.
- [32] D. Wang, D. Tan, and L. Liu, "Particle swarm optimization algorithm: An overview," *Soft Comput.*, vol. 22, pp. 387–408, Jan. 2018.
- [33] Y. Zhang, X. Liu, F. Bao, J. Chi, C. Zhang, and P. Liu, "Particle Swarm Optimization with Adaptive Learning strategy," *Knowl. Based Syst.*, vol. 196, May 2020, Art. no. 105789.
- [34] C. Huang and J. Fei, "UAV path planning based on particle swarm optimization with global best path competition," *Int. J. Pattern Recognit. Artif. Intell.*, vol. 32, no. 6, 2018, Art. no. 1859008.
- [35] M. D. Phung and Q. P. Ha, "Safety-enhanced UAV path planning with spherical vector-based particle swarm optimization," *Appl. Soft Comput.*, vol. 107, Aug. 2021, Art. no. 107376.
- [36] G. Xu et al., "Particle swarm optimization based on dimensional learning strategy," *Swarm Evol. Comput.*, vol. 45, pp. 33–51, Mar. 2019.
- [37] Z. Qadir, M. H. Zafar, S. K. R. Moosavi, K. N. Le, and M. P. Mahmud, "Autonomous UAV path-planning optimization using metaheuristic approach for predisaster assessment," *IEEE Internet Things J.*, vol. 9, no. 14, pp. 12505–12514, Jul. 2022.
- [38] Q. Hou, Y. Cai, Q. Hu, M. Lee, and G. Yu, "Joint neural network for trajectory and communication design in multi-UAV systems," in *Proc. IEEE Global Commun. Conf. (GLOBECOM)*, Dec. 2022, pp. 2182–2187.
- [39] Y. Zeng, J. Xu, and R. Zhang, "Energy minimization for wireless communication with rotary-wing UAV," *IEEE Trans. Wireless Commun.*, vol. 18, no. 4, pp. 2329–2345, Apr. 2019.
- [40] A. Al-Hourani, S. Kandeepan, and S. Lardner, "Optimal LAP altitude for maximum coverage," *IEEE Wireless Commun. Lett.*, vol. 3, no. 6, pp. 569–572, Dec. 2014.
- [41] S. Shao, Y. Peng, C. He, and Y. Du, "Efficient path planning for UAV formation via comprehensively improved particle swarm optimization," *ISA Trans.*, vol. 97, pp. 415–430, Feb. 2020.



**YULIN ZHOU** (Member, IEEE) received the M.E. and Ph.D. degrees in electronics engineering from the University of Warwick, Coventry, U.K., in 2016 and 2019, respectively. He is currently working as a Lecturer with the Ningbo Innovation Center, Zhejiang University, China. His research interests include wireless communications, performance analysis, channel estimation, wireless relaying, UAV communications, and energy harvesting.



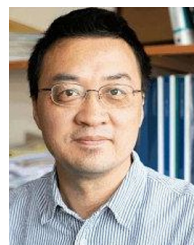
**AZIZ ALTAF KHUWAJA** received the B.E. degree in telecommunication engineering from the Mehran University of Engineering and Technology, Jamshoro, Pakistan, in 2010, the M.Sc. degree in electronics communication and computer engineering from the University of Nottingham, Nottingham, U.K., in 2015, and the Ph.D. degree in engineering from the University of Warwick, Coventry, U.K., in 2021. He is currently an Assistant Professor with the Department of the Electrical Engineering, Sukkur IBA University, Pakistan. His research interest includes wireless communication and signal processing.



**XIAOTING LI** (Member, IEEE) received the B.S. and M.E. degrees in electronics engineering from Zhejiang University, China, in 2021 and 2024, respectively. Her research interests include wireless communications, performance analysis, channel estimation, and UAV communications.



**NAN ZHAO** (Senior Member, IEEE) received the Ph.D. degree in information and communication engineering from the Harbin Institute of Technology, Harbin, China, in 2011. He is currently a Professor with the Dalian University of Technology, China. He won the Best Paper Awards in IEEE VTC in Spring 2017, ICNC in 2018, WCSP in 2018, and WCSP in 2019. He also received the IEEE Communications Society Asia Pacific Board Outstanding Young Researcher Award in 2018. He is serving on the editorial boards for IEEE WIRELESS COMMUNICATIONS, IEEE WIRELESS COMMUNICATIONS LETTERS, and IEEE TRANSACTIONS ON GREEN COMMUNICATIONS AND NETWORKING.



**YUNFEI CHEN** (Senior Member, IEEE) received the B.E. and M.E. degrees in electronics engineering from Shanghai Jiaotong University, Shanghai, China, in 1998 and 2001, respectively, and the Ph.D. degree from the University of Alberta in 2006. He is currently working as a Professor with the Department of Engineering, University of Durham, U.K. His research interests include wireless communications, performance analysis, joint radar communications designs, cognitive radios, wireless relaying, and energy harvesting.